

Specific proteolysis mediated by a p97-directed proteolysis-targeting chimera (PROTAC)

Constanza Salinas-Rebolledo¹, Javier Blesa², Guillermo Valenzuela-Nieto¹, David Schwefel³,
Natalia López González del Rey², Maxs Méndez-Ruette⁴, Janine Burkhalter¹, Luis Federico Bátiz⁵
&⁶, Ronald Jara¹, José A. Obeso², Pedro Chana-Cuevas⁷, Gopal P. Sapkota⁸, Alejandro Rojas-
Fernandez^{1,9&10#}

1 Institute of Medicine and Center for Interdisciplinary Studies on the Nervous System, CISNE, Faculty of Medicine, Universidad Austral de Chile, Valdivia, Chile.

2 HM CINAC (Centro Integral de Neurociencias Abarca Campal), Hospital Universitario HM Puerta del Sur, HM Hospitales, Madrid, Spain

3 Technische Universität Berlin, Chair of Bioanalytics, 10623 Berlin, Germany

4 Programa de Doctorado en Biomedicina, Facultad de Medicina, Universidad de los Andes

5 Neuroscience Program, Centro de Investigación e Innovación Biomédica (CiiB) & School of Medicine, Facultad de Medicina, Universidad de los Andes, Santiago, Chile.

6 IMPACT, Center of Interventional Medicine for Precision and Advanced Cellular Therapy, Santiago, Chile.

7 CETRAM & Faculty of Medical Science Universidad de Santiago de Chile, Chile.

8 Medical Research Council Protein Phosphorylation and Ubiquitylation Unit, School of Life Sciences, University of Dundee, Sir James Black Centre, Dundee, UK

9 Berking Biotechnology SpA, Valdivia, Chile & Berking Bioscience GmbH, Hamburg, Germany

Correspondence should be addressed to alejandro.rojas@uach.cl

Abstract

The p97 protein is a member of the AAA + family of ATPases. It is a mechanoenzyme that uses energy from ATP hydrolysis to promote protein unfolding and segregation actively. The unfolded products of p97 are presented to the 26S Proteasome for degradation. p97 substrate recognition is mediated by adaptors, which interact with substrates directly or indirectly through ubiquitin modifications, resulting in substrate funnelling into the central pore of the p97 hexamer and unfolding. We have engineered synthetic adaptors to target specific substrates to p97, using the extraordinary intracellular binding capabilities of camelid nanobodies fused to the UBX domain of the p97 Adapter FAF1. In such a way, we created a p97-directed proteolysis-targeting chimera (PROTAC), representing a unique E3 ubiquitin ligase-independent strategy to promote specific proteolysis.

Introduction

The ubiquitin-proteasome system (UPS) regulates protein abundance by specific E3 ubiquitin ligases, which catalyze ubiquitin chain formation on the substrates, inducing their proteasome-mediated degradation¹⁻⁴. The UPS as an efficient natural negative-regulatory mechanism has inspired the development of the Proteolysis-Targeting Chimera (PROTAC) technology, involving synthetic heterobifunctional molecules able to recruit a protein of interest (POI) to a ubiquitin E3 ligase to induce its proteasomal degradation^{5-16,17,18}.

The nature of PROTACs varies from small molecules to protein domains and antibody fragments. Several camelid Nanobodies are capable of binding intracellular target proteins selectively, with a high affinity. When Nanobodies are overexpressed in cells, they are also known as intrabodies^{15,19,20}. Nanobodies fused to ubiquitin E3 ligase substrate receptors trigger protein degradation of ectopic and endogenous targets. For instance, the AdPROM system consisting of a fusion of the E3 substrate receptor VHL with nanobodies against a range of POIs leads to the efficient degradation of endogenous POI targets^{8,9,20-24}. Nanobodies have also been engineered

and fused directly to the active domains of Ubiquitin E3 ligases, such as the antibody RING-mediated destruction system (ARMeD), which uses the RING finger domain of the Ubiquitin E3 ligase RNF4 fused to a nanobody. A valuable feature of the ARMeD system is its independence of the endogenous ubiquitin E3 ligases¹⁵.

In addition to conventional ubiquitination and proteasomal-mediated degradation, the AAA-type ATPase p97 assists the proteasome in the specific selection of substrate degradation in eukaryotic cells²⁵. The key mechanism of action of p97 is the disassembly of protein complexes²⁶ through its ATP-dependent *segregase* and *unfoldase* activity²⁷⁻²⁹. p97 uses ATP hydrolysis as a source of energy to 'segregate' ubiquitylated protein complex subunits from their binding partners, or even for the unfolding of protein aggregates^{30,31}, such as tau amyloid fibers³² and Huntingtin Exon 1³³. This action is mediated by two types of adapters: the UBX-like domain (UBX-L, also known as the "ubiquitin-binding domain" [UBD]) adapters such as Ufd1, NLP4, p47, FAF1, SAKS, UBXD7 and UBXD8, and the UBX-only adapters, such as p37, UBXD1, UBXD2, UBXD3, UBXD4, UBXD5, UBXD6, VCIP135 and YOD1³⁴⁻³⁸. p97 regulates ER-mitochondrial association by disassembling Mfn2 complexes upon PINK/Parkin phosphoubiquitination³⁹ and the mitochondrial extraction of MARCH5⁴⁰. It also co-localizes with protein aggregates involved in several neurodegenerative diseases, suggesting that p97 *segregase* and *unfoldase* activities could be related to the proteolytic control of proteins of therapeutic interest⁴¹⁻⁴⁶. For instance, p97 is recruited to poly-Q aggregates *in vitro*³¹ and to inclusion-positive neurons in Huntington's disease patients⁴². Abnormal protein aggregation is observed in several pathologies such as body myopathy associated with Paget's disease, frontotemporal dementia^{47,48}, Charcot–Marie–Tooth disease⁴⁹, amyotrophic lateral sclerosis⁵⁰, and Parkinson's disease⁴⁶. Ubiquitin is often found as a resident protein within aggregates related to neurodegenerative diseases suggesting potential dysfunction of ubiquitin-mediated degradation signaling⁵¹⁻⁵⁴.

Motivated by these characteristics, we engineered a synthetic p97 adapter by fusing the UBX domain of the FAF1 protein to camelid nanobodies, to assemble a novel p97-based PROTAC

technology (**p97-PROTAC**). This new chimera efficiently targets proteins for segregation and proteasome-mediated degradation in a ubiquitin-independent manner.

Results

p97-PROTAC subcellular recruitment and activity in cells

p97 adapters and cofactors lead to the specific recognition of ubiquitin-modified and unmodified substrates along with simultaneous entry into the central pore of p97 hexamers, followed by unfolding and subsequent proteasomal degradation^{55,56}. We hypothesized that p97 adapters could be engineered to target non-natural substrates of clinical interest for degradation. Thus, we generated a synthetic chimera consisting of the Ubx domain of the p97 adapter FAF1 fused via a linker to a GFP-specific camelid nanobody (Ubx-Nb^(GFP)), which is capable of recognizing both GFP and YFP tagged proteins⁵⁷, to yield a novel PROTAC based on p97 activity (Figure 1A). Using fluorescence microscopy, we then evaluated if the Ubx-Nb^(GFP) recognizes GFP-fusion proteins with different sub-nuclear localization by analyzing Ubx-Nb^(GFP) recruitment to a group of differentially located targets: i) GFP-Coilin (Nuclear and Cajal Bodies), ii) GFP-Emerin (a type II integral membrane protein residing principally at the inner nuclear membrane), and ii) GFP-ETV1 (Nuclear transcription factor) in HeLa cells. We observed efficient Ubx-Nb^(GFP) recruitment to diverse nuclear locations (Figure 1B).

Next, we studied the effect of Myc-tagged Ubx-Nb^(GFP) PROTAC expression on the levels of GFP-Coilin, GFP-Emerin and GFP-ETV1. We observed a significant reduction in the levels of all GFP target proteins with increasing amounts of Myc-Ubx-Nb^(GFP), indicating that the p97-PROTAC - Ubx-Nb^(GFP), is sufficient to trigger specific proteolysis of target proteins (Figure 1C-1H). Consistently, no degradation was observed when the GFP nanobody was replaced by a negative control nanobody (Supplementary Figure 1A-C). Therefore, this suggested that p97-PROTAC could be an alternative targeted protein degradation (TPD) approach to the conventional ubiquitin ligase-based PROTACs and might be useful for the degradation of large protein

complexes, integral membrane protein at the inner nuclear membrane and toxic aggregates due to its *unfoldase* and *segregase* activities.

Specific degradation of proteins within liquid-liquid phase separation structures

We sought to test the efficacy of the p97-PROTAC system for the degradation of proteins whose expression was driven by endogenous promoters. To further interrogate the p97-PROTAC for its ability to induce degradation of proteins within aggregates and packed in highly condensed regions, we chose *53BP1* as the target protein, as it is a well-known component of liquid-liquid phase separation structures (LLPS)^{58,59}.

First, we generated a knock-in cell line by fusing a yellow fluorescent protein to the N-terminus of the endogenous *53BP1* protein using CRISPR/Cas9 technology. 24h after transfection with a forward and reverse gRNA and the donor vector, Cas9 D10A nickase was induced with doxycycline. Single YFP-positive cell clones were isolated by cell sorting (Figure 2A). Natural DNA damage that occurs during DNA replication induces the accumulation of *53BP1* Fluorescence signal in distinct nuclear foci. The foci are typical for *53BP1*, which has been described to accumulate in nuclear bodies during the G1 phase of the cell cycle⁶⁰. The YFP-*53BP1* Knock-In (KI) clones were analyzed by fluorescence microscopy and a heterozygote clone was selected (Figure 2B). We characterized *53BP1* foci in U2OS YFP-*53BP1* (KI) cells by structured illumination microscopy (SIM) (Figure 2C). Further, we evaluated the localization of the YFP-*53BP1* KI and endogenous *53BP1* by SIM microscopy and demonstrated the expected location for the knock-in fusion (Figure 2D). Accordingly, the YFP-*53BP1*(KI) cell line fully recapitulated the localization of endogenous *53BP1* and the endogenous *53BP1* promoter controls the YFP-*53BP1* KI expression. *53BP1* nuclear bodies have been described as membrane-less organelles, organized by liquid-liquid phase separation (LLPS)^{58,59}. Hence, we used the YFP-*53BP1* KI cells as a model to study the recruitment and function of the p97-PROTAC *Ubx-Nb*^(GFP) to target LLPS. We observed that the *Ubx-Nb*^(GFP) construct was successfully recruited to nuclear foci characterized by the *53BP1*

location (Figure 2E). Importantly, Ubx-Nb^(GFP) expression significantly reduced 53BP1 levels, suggesting that our p97-PROTAC technology can specifically trigger the degradation of proteins within LLPS compartments (Figure 2F & 2G).

Endogenous p97 expression in the brain

Conventional PROTAC technologies exploit the activity of E3 ubiquitin ligases and accordingly require the expression of a suitable ligase to cause target ubiquitination and degradation. Likewise, the p97-PROTAC function requires the endogenous p97 expression. Therefore, we studied the expression of p97 in the brains of animal models. We observed ubiquitous expression in the cortex of non-human primates (NHPs), mice and rats. Endogenous p97 expression was observed in the hippocampus and substantia nigra pars compacta (SNpc) in mice and rats, the major pathological sites in Alzheimer's⁶¹ and Parkinson's disease respectively⁶² (Figure 3). Unfortunately, no tissue of NHP was available for other brain regions. Thus, p97 is endogenously expressed in regions of clinical interest that are affected by neurodegenerative diseases. Ultimately, the segregase and *unfoldase* activity of p97 in the brain could be advantageous for p97-PROTAC-based targeted degradation of toxic protein aggregates, especially for neurodegenerative diseases.

Structural superposition of p97, Ubx, Nb^(GFP) and GFP

To gain insight into the structure of substrate-bound p97-PROTAC in the context of the p97 assembly, an AlphaFold2-based model of the p97-PROTAC/GFP-complex bound to p97 was generated (Figure 4A) (see Methods for details of the modelling procedure). After manually adjusting the conformation of the flexible linker between PROTAC Ubx and Nb^(GFP) moieties, the model shows that PROTAC-recruited GFP can access the central p97 pore (<15 Å distance between the pore entrance and the closest GFP residue) (Figure 4A & 4B). Consistent with the model, we determined that GFP alone, a barrel conformation protein of 28 kDa, can be recruited

by the p97-PROTAC and is efficiently processed for degradation (Figure 1B, 4C & 4D). To test the mechanism by which the GFP became degraded, we co-transfected cells with GFP and either, an empty vector or with the p97-PROTAC Ubx-Nb^(GFP). After 20h, cells were treated with the proteasome inhibitor MG132 or DMSO as control. Upon MG132 treatment, we observed a full rescue of GFP protein levels. Therefore, by using a small substrate such as GFP as a model, we demonstrated that p97-PROTAC proteolytic activity relies on proteasome-mediated degradation (Figure 4E & 4F). Furthermore, upon depletion of p97 by siRNA transfection (Figure 4G), a significant rescue of GFP-Emerin protein levels was observed (Figure 4H), concomitant with an increase of the levels of the p97-PROTAC Ubx-Nb^(GFP) (Figure 4I), indicating that the PROTAC Ubx-Nb^(GFP) itself is also a substrate of the p97. To test the hypothesis that p97-PROTAC action is a ubiquitination-independent process, we globally inhibited ubiquitination using PYR41, a cell-permeable, irreversible inhibitor of the ubiquitin-activating enzyme E1 activity. First, we demonstrated that PYR41 was able to stabilize p53 in HeLa cells (Supplemental Figure 1D). Next, we used GFP-Emerin as a substrate model and treated the cell with either DMSO or 50uM of PYR41 for 4h, and in accordance with our hypothesis, no inhibition of GFP-Emerin degradation was observed by the PYR41 treatment (Figure 4J & 4K). We also investigated whether the activities of p97 were required for the substrate mediated degradation triggered by p97-PROTAC Ubx-Nb^(GFP). We tested the degradation of GFP-Emerin in HeLa cells treated with either DMSO or CB-5083, a potent inhibitor of the ATPase activity of p97. As an internal control, we measured the levels of CHOP, a sensor of ER stress known to be induced by p97 inhibitors (Figure 4L). Surprisingly we did not observe inhibition of degradation of GFP-Emerin in cells treated with CB-5083, despite a slight increase in CHOP levels (Figure 4M). Thus, our results show that p97-PROTAC targets proteins for proteasomal mediated degradation by a ubiquitin-independent mechanism.

Degradation of proteins of clinical interest by a p97-based PROTAC

A hallmark for several neurodegenerative diseases is the accumulation of toxic aggregates in the intra- or extracellular space⁶³. PROTAC technology has the potential to become a new therapeutic approach for proteotoxic diseases⁶⁴. High levels of ubiquitin are found in intracellular aggregates, suggesting that ubiquitination-mediated proteasome degradation may be partially impaired^{65,66}. Targeting p97 to toxic aggregates can potentially contribute to the clearance of aggregates by inducing segregation, unfolding, and proteasomal degradation simultaneously. We tested two aggregate models of clinical interest for p97-PROTAC-mediated degradation, Huntingtin and α -Synuclein. In the first experiment, we used a GFP-fusion plasmid containing the exon 1 of HTT with either 23 CAG repeats (GFP-HTT Q23, wild-type HTT) or 74 CAG repeats (GFP-HTT Q74, mutant HTT)⁶⁷. We observed efficient degradation of GFP-HTT Q23 by the p97-PROTAC Ubx-Nb^(GFP) (Figure 5A & 5B) and a co-localization of p97-PROTAC Ubx-Nb^(GFP) with HTT GFP-HTT Q23 (Figure 5C). Subsequently, we repeated the experiment to test the degradation of GFP-HTT Q74 and observed aggregate formation after mutant HTT transfection concomitant with efficient degradation of GFP-HTT Q74 by the p97-PROTAC Ubx-Nb^(GFP) (Figure 5D-F).

In the second challenge, we tested the capability of the p97-PROTAC Ubx-Nb^(GFP) to mediate the degradation of a GFP-tagged α -Synuclein mutant A53T and observed efficient degradation (Figure 6A & 6B). Then we generated another p97-PROTAC by replacing the anti-GFP nanobody with a specific α -Synuclein nanobody (NbSyn87)⁶⁸⁻⁷¹. Likewise, cells were transfected with an untagged α -Synuclein A53T mutant together with an empty vector (as control) or with increasing concentrations of the anti- α -Synuclein p97-PROTAC Ubx-Nb^(Syn87). Again, we observed efficient degradation of the α -Synuclein A53T p97-PROTAC (Figure 6C & 6D). Thus, we demonstrated that the nanobody component on the p97-PROTAC is exchangeable and that the p97-PROTAC system is suitable for degrading human proteins of clinical interest.

Discussion

The constitutive degradation of proteins is a rapid negative-regulatory mechanism, often involved in important stress response pathways. For example, under normoxia, Hif1 α is rapidly hydroxylated in an oxygen-dependent manner, and the hydroxylation is recognized by an E3 Ligase receptor called VHL leading to continuous ubiquitin-mediated proteasomal degradation^{73,75-77}. Hypoxia decreases Hif1 α hydroxylation, and consequently, Hif1 α dissociates from VHL, resulting in rapid stabilization, accumulation, and activation of the hypoxia response. Therefore, endogenous degradation is a natural and efficient way to downregulate the amount and function of proteins.

PROTAC technologies today rely on ubiquitin-mediated proteasomal degradation, but abnormal protein aggregation has multiple detrimental effects in the ubiquitin-mediated proteasomal degradation, including a significant reduction of the free ubiquitin pool⁷⁸ and abundant ubiquitin accumulation into proteotoxic aggregates. Our p97-PROTAC technology provides an alternative to ubiquitin-mediated degradation.

We showed that an engineered p97-PROTAC consisting of a Ubx domain fused to a camelid nanobody was sufficient to trigger specific protein degradation in cells and further, using the ubiquitin E1 inhibitor PYR41, we demonstrated that p97-PROTACs are not inhibited by ablation of ubiquitination. In addition, using siRNA specific against p97, we inhibited the degradation of the substrate model. Intriguingly, we could not inhibit the action of p97-PROTACs with the specific p97 ATPase inhibitor CB-5083. Thus, mechanistically we cannot distinguish if the p97-PROTACs overcame the effect of the inhibitor or if the degradation mediated by the p97-PROTACs is mediated only by induced proximity to the proteasome and independent of p97's ATPase activity. Further experiments need to be performed to understand the mechanism by which p97-PROTACs mediate ubiquitin-independent degradation in cells.

p97 is an extensively characterized ubiquitously expressed protein involved in fundamental cellular processes, such as the degradation of proteins associated with the endoplasmic reticulum

(ER) (ERAD)⁷⁹, autophagy⁸⁰, and it is also an important player in the proteostasis of aggregates in Parkinson's disease^{46,81,82}. Indeed, p97 has been shown to protect against the proteopathic spread of pathogenic aggregates in animal models⁸³. In this study, we characterized p97 expression in the brains of animal models and observed ubiquitous p97 expression in all sections. Specifically, high p97 expression levels were detected in the cortex, substantia nigra pars compacta and hippocampus, regions highly prone to protein aggregation and neurodegeneration in neurodegenerative diseases such as Parkinson's and Alzheimer's disease⁶³. These observations support the possibility of using p97-based PROTACs to reduce protein aggregation in neurodegeneration-related targets in the future.

The PROTAC technologies might increase the number of druggable proteins by a change in the inhibition paradigm. In contrast to conventional drugs that aim for chemical modulation of the enzymatic activity or function, PROTAC aims at the downregulation of the levels of specific targets based exclusively on selective binding and degradation.

In conclusion, our work unveils the potential of a p97-PROTAC as the first E3 ubiquitin ligase-independent technology that targets proteins for degradation at diverse subcellular locations, integral membrane protein residing at the inner nuclear membrane, chromatin located and liquid-liquid phase separated compartments, also providing a new technology to target protein aggregates of clinical interest for proteasomal degradation.

Material and Methods

Design and cloning

The constructs consist mainly of three domains: an anti-GFP nanobody²⁰, which binds to the target protein; a linker and the UBX domain of the p97 Adapter FAF1. The linker used to connect both

domains, KESGSVSSSEQLAQFRSLD, was originally designed for the construction of single-chain antigen-binding proteins, connecting its constituent domains with sufficient flexibility to avoid hindering its antigen-binding capacity⁸⁵. Anti-GFP nanobody can recognize both, the YFP and GFP protein.⁵⁷ In addition, a myc-tag was added to prove expression. The full sequence was cloned into the pcDNA 5 FRT/TO vector by the Gibson Assembly technique. Later, the anti-GFP nanobody was cut with restriction enzymes to be replaced by an anti- α -Synuclein (Nb87) nanobody NbSyn87⁶⁸⁻⁷¹.

Cell culture

All cells (HeLa and U2OS) were cultured in Dulbecco's Modified Eagle's medium (DMEM; Gibco) supplemented with 10% fetal bovine serum and 100 units/mL of penicillin and streptomycin and maintained at 37°C in a humidified incubator at 5% CO₂. Plasmid transfection was performed in 6-well plates using 4 μ g of DNA, 24 h after transfection, cells were lysed, and proteins were collected. Cells were transiently transfected with the following vectors: pcDNA5 FRT/TO GFP-ETV1, pcDNA5 FRT/TO GFP-Emerin, pEYFP-Coilin, pcDNA FRT/TO GFP, pEGFP-C1-tagged plasmids containing the exon 1 of HTT with 23 CAG repeats (GFP-Q23: wild-type HTT. Addgene, #40261) or 74 CAG repeats (GFP-Q74: mutant HTT. Addgene, #40262). Vectors to alpha synuclein were a gift from our collaborator Dr. Gopal Sapkota (pcDNA5-FRT/TO-GFP-SCNA-A53T, #59047 or pcDNA5-FRT/TO-SCNA-A53T, #59042). As control, we used an empty vector pcDNA5 FRT/TO. Transfection was performed using Lipofectamine 2000 (Invitrogen) according to the manufacturer's instructions, and media were supplemented with normocin (100 ug/mL) during transfection (Invivogen). For lysis, cells were washed twice in ice-cold phosphate buffer saline (PBS), scraped on ice in lysis buffer (Tris-HCl pH 6.8, NaCl, glycerol and SDS 10%), supplemented with complete protease inhibitors (one tablet per 25 mL: Roche), and 0.1% b-mercaptoethanol (Sigma). Cell extracts were either cleared and processed immediately or stored

at -20°C. The protein concentration was determined in a 96-well format using the Pierce BCA protein assay kit (Thermo Fisher Scientific).

Antibodies & Inhibitors

We used the following primary antibodies; anti-GFP (Invitrogen, GF28R mAb MA5-15256), anti- α -Synuclein (Santa Cruz Biotechnology, 3H2897 mAb sc-69977), anti-53BP1 (Invitrogen, 53BP1 Polyclonal Antibody PA1-16565), anti-Myc-tag (Cell Signaling, 9B11 Mouse mAb #2276), anti-vcp/p97 (Sigma-Aldrich Polyclonal Antibody HPA012728), anti-p53 (Invitrogen, monoclonal antibody DO-7 # MA5-12557), anti-CHOP (Cell Signaling, L63F7 Mouse mAb #2895), anti-ubiquitin (Sigma-Aldrich ST1200 Mouse mAb FK2), anti-alpha Tubulin (Santa Cruz Biotechnology, B7 mAb sc-5286), anti-GAPDH (Santa Cruz Biotechnology, mAb sc-47724), anti-vinculin (Santa Cruz Biotechnology, 7F9 mAb sc-73614). Horseradish peroxidase (HRP)-coupled secondary antibodies and Alexa Fluor secondary antibodies were purchased from Invitrogen (ThermoFisher): Mouse IgG, IgM (H+L) Secondary Antibody (A-10677), Rabbit IgG (H+L) Secondary Antibody (31460) and Mouse IgG (H+L) Highly Cross-Adsorbed Secondary Antibody (A-11032).

The inhibitors used in this work were: MG132, a proteasome inhibitor from Sigma-Aldrich (catalog number 474790); PYR-41, an E1 ligase inhibitor from Sigma-Aldrich (catalog number N2915); and CB-5085, a D2 domain inhibitor of p97 from Cayman Chemical.

Generation of a 53BP1 endogenously tagged YFP-53BP1 using CRISPR/Cas9

U2OS T-Rex cells were co-transfected with the pOG44 plasmid, which constitutively expresses the Flp recombinase and pcDNA5 FRT/TO codon optimized Streptococcus pyogenes M1 GAS Cas9 D10A-NLS-FLAG (DU45732 MRC-PPU reagent) for isogenic integration of the cassette. To decrease possible off-target effects, we applied the CAS9 D10A nickase system for genetic cleavage. Single clones were selected to generate the U2OS stable expressing Cas9 D10A cells, U2OS SEC-C D10A. Two specific guide RNA (gRNA) targeting sequences were identified in the

5'UTR before the 53BP1 start codon using the E-CRISPR software (http://www.e-crisp.org/E-CRISP/reannotate_crispr.html). The forward gRNA g53BP1-1 5'AGACCTCTAGCTCGAGCGCGAGG 3' and a reverse gRNA g53BP1-7 5'GTCCCTCCAGATCGATCCCTAGG 3' were cloned into pU6-Puro via site-directed mutagenesis using the QuickChange method (Stratagene) cloned using the previously described methodology^{86,87} and confirmed by DNA sequencing. We designed a strategy for YFP delivery at the N-terminus of the 53BP1 protein using a CRISPR/Cas9 knock-in methodology. In short, the sense and antisense gRNAs were transfected in U2OS T-Rex cells and modified to produce Cas9 D10A nickase in a doxycycline-inducible manner. We also engineered a synthetic vector with two homologous flanking regions around the cleavage site, where we inserted YFP cDNA and small linker in front of the endogenous 53BP1 gene synthetically produced by GeneArt (Life Technologies) (supplemental methods). The gRNA recognition sites were mutated on the synthetic donor to avoid cleavage by the gRNA/Cas9 complex. Finally, the two gRNAs and the donor vector carrying the YFP cDNA flanked with the homologue regions were transfected in U2OS cells. The day after the cells were transfected, the expression of the Cas9 nuclease was induced by adding 1 µg/mL doxycycline and the cells were incubated for 4 days before FACS analysis to identify YFP positive cells and further cell sorting based on single cell isolation.

Flow cytometry and cell sorting

Cells were analyzed for YFP fluorescence on an LSR Fortessa or FACS Canto flow cytometer (Becton Dickinson) and data were analyzed using FlowJo software (Tree Star Inc). Single cells were identified based on FSC-A, FSC-W and SSC-A, and YFP fluorescence measured with 488 nm excitation and emission detected at 530±30 nm. Cell sorting was performed on an Influx cell sorter (Becton Dickinson) with FACS Software, using the same cell identification procedure described above. Single YFP expressing cells were sorted onto individual wells of a 96-well plate containing DMEM supplemented with 20% fetal bovine serum (FBS), 2 mM L-glutamine, 100

units/ml penicillin, 100 µg/ml streptomycin, and 100 µg/ml transfection compatible antibiotic normocin 1x (Invivogene). Single-cell clones were left to proliferate, and YFP fluorescence was determined.

Immunofluorescence and high content microscopy

HeLa cells transfected with GFP proteins were grown in a 96-well optical plate (Thermo Fisher Scientific) or 24-well lidded plates. Cells were fixed with 4% paraformaldehyde at 37°C for 10 min. Cells were washed with 1x PBS and permeabilized in 0.2% TritonX100 PBS. After washing the cells three times in 1x PBS, they were incubated with blocking solution (FBS 5%-PBS 1x) for 30 minutes and then incubated with the primary antibody for 1 hour at 37 ° C. After washing another three times with 1x PBS, a secondary antibody Alexa Fluor was used at 1: 3000, it was incubated for 45 min at 37 ° C. For nuclei staining, cells were washed with PBS and incubated for 10 min at room temperature with 0.1 mg / ml DAPI. After the final wash, the cells were kept in the 96-well optical plates in 1x PBS. Cover-fixed cells were mounted on slides. Fixed cell images were acquired with a high content automated microscope, Celldiscoverer 7 (Carl Zeiss GmbH, Jena, Germany).

Silencing assay

HeLa cells were cultured in a 6-well plate and transfected with siRNAs control siRNA-B, (sc-44230), or p97 siRNA (sc-37187) at 40% confluence. Transfection was performed using Lipofectamine RNAiMax (Invitrogen) according to the manufacturer's instructions, and the media were supplemented with Normocin (Invivogen) during transfection. Twenty-four hours post siRNA transfection, the medium was changed to fresh DMEM-Normocin, and GFP-Emerin, as well as both the empty vector and the [Ubx-Nb \(GFP\) vector](#), were co-transfected. The complexes were left in culture for 48 hours. Subsequently, total proteins were extracted with lysis buffer to perform the western blot assay.

SDS-PAGE and western blotting

Reduced protein extracts were separated on 10% SDS-PAGE gels or 4–12% NuPAGE bis–tris precast gels (Invitrogen) by electrophoresis. Proteins were then transferred onto nitrocellulose membranes (Millipore). Non-specific sites were blocked with blocking solution (PBS containing 0.1% Tween20 with 5% (w/v) non-fat milk) for 30 min at room temperature with agitation. The blocking solution was discarded, and membranes were incubated overnight at 4°C in 5% BSA PBS-T (PBS 1x containing 0.1% Tween20) with the appropriate primary antibodies. Membranes were then washed in PBS-T and incubated with HRP-conjugated secondary antibodies in 5% milk-PBS-T for 1 hour at room temperature, followed by 3 x 5 min washes with PBS-T and visualized using the ECL reagent (Pierce) and exposure on medical X-ray films.

Animals, fixation, and tissue processing

Mouse (C57BL6 / C mice), rat (sprague dawley), and monkey (*Macaca fascicularis*) brain sections were obtained from the brain bank of HM CINAC. All procedures with animals were carried out in accordance with the Directive of the Council of the European Communities (2010/63 / EU) and Spanish legislation (RD53 / 2013) on animal experimentation⁸⁸. Animal perfusion, fixation, and tissue processing was carried out as previously described^{88,89}.

Brain immunohistochemistry

Coronal free-floating 30-mm thick sections were washed with Tris buffer (TB) and treated with citrate buffer (pH 6) for 30 min at 37° C for antigen retrieval. Inhibition of endogenous peroxidase activity was carried out using a mixture of 10% methanol and 3% concentrated H₂O₂ for 20 min at room temperature. Normal serum of the same species as the secondary antibody (Normal Goat Serum, NGS) was applied for 3 h to block non-specific binding sites. The sections were

immunostained with anti-p97 antibody (Rabbit polyclonal anti-vcp, sigma aldrich HPA012728, dilution 1: 1000) at 4 ° C for 72h. The sections were washed with Tris-buffered saline (TBS) and incubated for 2 h with a solution containing the secondary biotinylated antibody (goat anti-rabbit, dilution 1:400; Chemicon, Burlington, USA) in TBS-NGS. The sections were then incubated for 45 min with the avidin-biotin-peroxidase complex (PK-6100, ABC Vectastain; Vector Laboratories, Burlingame, USA). Immunohistochemical reactions were visualized by incubating the sections with 0.05% 3,3-diaminobenzidine (DAB, Sigma, St. Louis, USA) and 0.003% H₂O₂. The sections were then dehydrated with graduated ethyl alcohol (EtOH) and rinsed in two xylene changes before being mounted in dibutyl polystyrene xylene phthalate (DPX) and applying glass coverslips. Omission of the primary antibody resulted in a lack of staining (images not shown).

Molecular modelling

An atomic model of *Ubx-Nb*^(GFP) was predicted using the AlphaFold2 algorithm via the ColabFold notebook^{90,91}. The FAF1 UBX domain position on the p97 hexamer was modelled by LSQ superposition of the p97 N-domain portion of a p97-N/FAF1 UBX co-crystal structure (PDB 3qq8)⁹² with the N-domain of chain A of a p97 hexamer cryo-EM structure (PDB 7jy5)⁹³ using the program Coot⁹⁴. Subsequently, the FAF1 UBX domain portion of the AlphaFold prediction was aligned with the p97/FAF1 UBX domain model using LSQ superpose in Coot. The conformation of the flexible linker between *Nb*^(GFP) and FAF1 UBX domain in the fusion protein model was manually adjusted using the “Regularize Zone” feature in Coot. Finally, the position of GFP was modelled by LSQ superposition of the nanobody portion of the adjusted *Ubx-Nb*^(GFP) coordinates with the crystal structure of a *Nb*^(GFP)/GFP co-crystal structure (PDB 3ogo)⁵⁷.

Statistical Analysis

The results are expressed as the mean ± SEM. All statistical analyses were performed using the GraphPad Prism software. For all western blots, an unpaired student's t-test was performed to

determine differences between control cells with an empty vector versus *Ubx* treated cells. A confidence level of 95% was accepted as significant.

Author Contributions Statement

Conceptualization: CSR, PCC and ARF; cloning and design: CSR, GVN, GPS and ARF; animal tissue acquisition, staining, and analysis: CSR, JB, NLGR, MMR, LFB, PCC and JO; immunofluorescence and microscopy images: CSR, JB and ARF; CRISPR/Cas9 editing ARF; biochemical studies and western blotting: C.S.R, structural modelling: D.S; analysis: CSR, LFB and ARF; funding acquisition PCC, JO and ARF; resources: PCC, JO and ARF; supervision: ARF; writing – original draft: CSR, PCC and ARF. All authors have contributed to writing, reviewing, and editing and have agreed to the published version of the manuscript.

Acknowledgments

This work was funded by FONDECYT REGULAR 1200427 to ARF; FONIS EU-LAC T010047 to CSR, PCC, JO, JB, NLR & ARF; to ARF; ANID- EXPLORACIÓN 13220075 to ARF & GVN; ANID 3220635 to GVN; MPG 190011 to ARF; ANID-STINT CS2018-7952. J.B was funded by ISCIII Miguel Servet Program CP19/00200 and FIS PI20/00496. Graduate fellowship ANID Nº 22170632 to C.S; N.L.G.R was funded by Becas Santander Iberoamerica Investigacion 2018/2019 and grant S2017/BMD-3700 (NEUROMETAB-CM) from Comunidad de Madrid; D.S. was supported by the German Research Foundation (DFG) Emmy Noether Programme SCHW1851/1-1. We would like to thank Anne Berking and Amber Philp for proofreading and Felipe Serrano for illustration.

Conflict of interest statement

The Austral University of Chile claiming priority to U.S. Provisional Patent Application No. US Serial No.63/326454

Figure Legends

Figure 1.- p97-mediated proteasome degradation. **A)** Diagram of p97 presenting ubiquitinated proteins to the proteasome via a UBX domain contacting adaptor (Top). p97-PROTAC system, consisting of a UBX domain fused to a nanobody (Nb) that recruits substrates for p97-mediated segregation, unfolding and proteasomal mediated degradation (Bottom). **B)** p97-PROTAC (UBX- $\text{Nb}^{(\text{GFP})}$) recognizes GFP tagged proteins at different cellular locations. HeLa cells were seeded on coverslip and co-transfected with UBX- $\text{Nb}^{(\text{GFP})}$ and GFP-Colin, GFP-Emerin and GFP-ETV1. Cells were fixed and we performed immunofluorescence for anti-myc tag to verify the expression of UBX- $\text{Nb}^{(\text{GFP})}$ and evaluated the colocalization. **C)** Western blot analysis of GFP-Coilin degradation by transfection with p97-PROTAC (UBX- $\text{Nb}^{(\text{GFP})}$), **D)** quantification of C; . **E)** Western blot analysis GFP-Emerin degradation by transfection with p97-PROTAC (UBX- $\text{Nb}^{(\text{GFP})}$), **F)** quantification of E; . **G)** Western blot analysis GFP-ETV1 degradation by transfection with p97-PROTAC (UBX- $\text{Nb}^{(\text{GFP})}$), **D)** quantification of G; Western blots were quantified and statistically analyzed using a student's t-test. $P < 0.05$ compared to controls. $n=3$.

Figure 2.- Targeting Liquid-liquid phase separation proteins by a p97-PROTAC. **(A)** Strategy for inserting a YFP tag on the N-terminus of the 53BP1 gene in U2OS SEC-C cells using CRISPR/Cas9 D10A. **B)** Selected Knock-In (KI) YFP-53BP1 clones isolated via flow cytometry. Clones were confirmed via fluorescence microscopy (GE Deltavision Widefield). **C)** Super-resolution images obtained with a Delta Vision OMX V4 structured illumination microscope (3D-

SIM). **D)** Immunofluorescence against 53BP1 (red) and colocalization with YFP-53BP1 in Knock-In cells. Images were obtained using a Delta Vision OMX V4 structured illumination microscope (3D-SIM). **E)** Recruitment of the p97-PROTAC UBX-Nb^(GFP) (Red) to YFP-53BP1 (green) within Liquid-liquid phase separation structures. Data were obtained with a High-content Celldiscoverer 7. UBX-Nb^(GFP) was detected using its myc-tag. **F)** Western blot analysis YFP-53BP1 degradation by UBX-Nb^(GFP) transfection in the knock-In U2OS cells, **G)** Quantification of F. Western blots were quantified and statistically analyzed using a student's t-test. P < 0.05 compared to controls. n=3.

Figure 3.- Endogenous p97expression in brain tissue. Immunohistochemistry against p97 in brain tissue sections from Non-Human Primates (Nhp) *Macaca fascicularis*, rat (*Sprague Dawley*) and mouse (C57BL6/C). p97 expression was detected in substantia nigra (SNpc), hippocampal, and cortical neurons. n=4

Figure 4.- Molecular model and degradation activity of p97-PROTAC. **A)** Model representations of the FAF1 UBX domain (purple), UBX-Nb^(GFP) (blue), GFP (green), and the p97 hexamer (light grey cartoon with semi-transparent molecular surface representation). **B)** A magnified view of the model shown in A. **C)** GFP monomer was co-transfected with UBX-Nb^(GFP) or empty vector in HeLa cells. Protein degradation was analyzed by western blot analysis. **D)** Quantification of C. **E)** GFP monomer was co-transfected with UBX-Nb^(GFP) or empty vector in HeLa cells, after 24 h were incubated with DMSO or the proteasome inhibitor MG132 (25 uM final concentration) for 4h. Protein degradation was analyzed by western blot. **F)** Quantification of E. **G)** p97 was silenced by transfection with p97-siRNA in HeLa cells. Subsequently, the cells were transfected with GFP-Emerin and either the empty vector or UBX-Nb^(GFP) vector. Protein degradation was analyzed western blot analysis. **H)** Quantification of GFP-Emerin in cells treated with the UBX-Nb^(GFP) vector in HeLa cells treated with either and siNT control or an SiRNA p97 siRNA. **I)** Quantification of the UBX-Nb^(GFP) in cells treated with the UBX-Nb^(GFP) vector in HeLa

cells treated with either and siNT control or an SiRNA p97 **J)** HeLa cells co-transfected with GFP-Emerin and either empty vector or UBX-Nb^(GFP) in addition the cells were treated with the E1 ubiquitin inhibitor PYR-41 (50 μ M) for 4 hours at 37°C. Subsequently, total proteins were extracted, and protein degradation was analyzed by western blot. **K)** Quantification of J. **L)** GFP-Emerin was co-transfected with UBX-Nb^(GFP) or empty vector in HeLa cells, after 24 h the cells were incubated with DMSO (as control) or the p97 inhibitor CB-5083 (4 μ M final concentration) for 6h. Protein degradation was analyzed by western blot using total proteins. **M)** Quantification of L. Western blots were quantified and statistically analyzed using a student's t-test. $P < 0.05$ compared to controls. $n=3$.

Figure 5.- Degradation of Huntington wild type and mutant with p97-PROTAC UBX-Nb^(GFP).
HeLa cells were transiently co-transfected with HTT GFP-tagged plasmids containing either 23 CAG repeats (GFP-HTT^{Q23} - wild-type HTT) or 74 CAG repeats (GFP-HTT^{Q74}: mutant HTT) **A)** HeLa cells co-transfected with GFP-HTT^{Q23} and increasing amount of the p97 PROTAC UBX-Nb^(GFP), degradation was determined by western blot analysis **B)** quantification of A; **C)** colocalization of GFP-HTT^{Q23} and p97 PROTAC UBX-Nb^(GFP) **D)** HeLa cells were co-transfected with GFP-HTT^{Q74} and increasing amount of the p97 PROTAC UBX-Nb^(GFP), degradation was determined by western blot analysis **E)** quantification of D; **F)** colocalization of GFP-HTT^{Q23} and p97 PROTAC UBX-Nb^(GFP). Western blots were quantified and statistically analyzed using a student's t-test. $P < 0.05$ compared to controls. $n=3$.

Figure 6.- Degradation of Alpha Synuclein with p97-PROTAC. **A)** HeLa cells were co-transfected with a vector expressing α Synuclein mutant A53T fused to GFP (GFP- α Synuclein A53T) and empty or increasing concentrations of UBX-Nb^(GFP). A53T-GFP degradation was determined by Western blot. **B)** Quantification of A. **C)** Cells were co-transfected with a vector expressing untagged alpha synuclein mutant A53T and an empty vector or increasing

concentrations of UBX-Nb^(Syn⁸⁷). Untagged α Synuclein A53T degradation was determined by Western blot using an anti α Synuclein antibody. **D)** Quantification of C. **E)** Representative model of p97-PROTAC functioning in the degradation of proteins and protein aggregates. Western blots were quantified and statistically analyzed using a student's t-test. $P < 0.05$ compared to controls. $n=3$.

References

1. Tara CS, Stanley JA, Kucera LS, Hollis S. Photodynamic inactivation of herpes simplex keratitis. *Arch Ophthalmol*. Jul 1974;92(1):51-3. doi:10.1001/archopht.1974.01010010055013
2. Ciechanover A. The ubiquitin-proteasome proteolytic pathway. *Cell*. Oct 7 1994;79(1):13-21. doi:10.1016/0092-8674(94)90396-4
3. McNaught KS, Olanow CW, Halliwell B, Isacson O, Jenner P. Failure of the ubiquitin-proteasome system in Parkinson's disease. *Nat Rev Neurosci*. Aug 2001;2(8):589-94. doi:10.1038/35086067
4. Schmidt MF, Gan ZY, Komander D, Dawson G. Ubiquitin signalling in neurodegeneration: mechanisms and therapeutic opportunities. *Cell Death Differ*. Feb 2021;28(2):570-590. doi:10.1038/s41418-020-00706-7
5. Bondeson DP, Mares A, Smith IE, et al. Catalytic in vivo protein knockdown by small-molecule PROTACs. *Nat Chem Biol*. Aug 2015;11(8):611-7. doi:10.1038/nchembio.1858
6. Sakamoto KM, Kim KB, Kumagai A, Mercurio F, Crews CM, Deshaies RJ. Protacs: chimeric molecules that target proteins to the Skp1-Cullin-F box complex for ubiquitination and degradation. *Proc Natl Acad Sci U S A*. Jul 17 2001;98(15):8554-9. doi:10.1073/pnas.141230798
7. Holland AJ, Fachinetti D, Han JS, Cleveland DW. Inducible, reversible system for the rapid and complete degradation of proteins in mammalian cells. *Proc Natl Acad Sci U S A*. Dec 4 2012;109(49):E3350-7. doi:10.1073/pnas.1216880109
8. Roth S, Macartney TJ, Konopacka A, et al. Targeting Endogenous K-RAS for Degradation through the Affinity-Directed Protein Missile System. *Cell Chem Biol*. Sep 17 2020;27(9):1151-1163 e6. doi:10.1016/j.chembiol.2020.06.012
9. Macartney TJ, Sapkota GP, Fulcher LJ. An Affinity-directed Protein Missile (AdPROM) System for Targeted Destruction of Endogenous Proteins. *Bio Protoc*. Nov 20 2017;7(22):e2614. doi:10.21769/BioProtoc.2614
10. Clift D, So C, McEwan WA, James LC, Schuh M. Acute and rapid degradation of endogenous proteins by Trim-Away. *Nat Protoc*. Oct 2018;13(10):2149-2175. doi:10.1038/s41596-018-0028-3
11. Békes M, Langley DR, Crews CM. PROTAC targeted protein degraders: the past is prologue. *Nat Rev Drug Discov*. Mar 2022;21(3):181-200. doi:10.1038/s41573-021-00371-6
12. Tomoshige S, Nomura S, Ohgane K, Hashimoto Y, Ishikawa M. Discovery of Small Molecules that Induce the Degradation of Huntingtin. *Angew Chem Int Ed Engl*. Sep 11 2017;56(38):11530-11533. doi:10.1002/anie.201706529
13. Tomoshige S, Ishikawa M. In vivo synthetic chemistry of proteolysis targeting chimeras (PROTACs). *Bioorg Med Chem*. Jul 1 2021;41:116221. doi:10.1016/j.bmc.2021.116221
14. Pankey GA. Infective endocarditis: changing concepts. *Hosp Pract (Off Ed)*. Mar 15 1986;21(3):103-10. doi:10.1080/21548331.1986.11704941
15. Ibrahim AFM, Shen L, Tatham MH, et al. Antibody RING-Mediated Destruction of Endogenous Proteins. *Mol Cell*. Jul 2 2020;79(1):155-166 e9. doi:10.1016/j.molcel.2020.04.032

16. Paiva SL, Crews CM. Targeted protein degradation: elements of PROTAC design. *Curr Opin Chem Biol.* Jun 2019;50:111-119. doi:10.1016/j.cbpa.2019.02.022
17. Wang Y, Jiang X, Feng F, Liu W, Sun H. Degradation of proteins by PROTACs and other strategies. *Acta Pharmaceutica Sinica B.* 2020/02/01/ 2020;10(2):207-238. doi:<https://doi.org/10.1016/j.apsb.2019.08.001>
18. Békés M, Langley DR, Crews CM. PROTAC targeted protein degraders: the past is prologue. *Nature Reviews Drug Discovery.* 2022/01/18 2022;doi:10.1038/s41573-021-00371-6
19. Caussinus E, Kanca O, Affolter M. Fluorescent fusion protein knockout mediated by anti-GFP nanobody. *Nat Struct Mol Biol.* Dec 11 2011;19(1):117-21. doi:10.1038/nsmb.2180
20. Fulcher LJ, Macartney T, Bozatzi P, Hornberger A, Rojas-Fernandez A, Sapkota GP. An affinity-directed protein missile system for targeted proteolysis. *Open Biol.* Oct 2016;6(10)doi:10.1098/rsob.160255
21. Fulcher LJ, Hutchinson LD, Macartney TJ, Turnbull C, Sapkota GP. Targeting endogenous proteins for degradation through the affinity-directed protein missile system. *Open Biol.* May 2017;7(5)doi:10.1098/rsob.170066
22. Simpson LM, Macartney TJ, Nardin A, et al. Inducible Degradation of Target Proteins through a Tractable Affinity-Directed Protein Missile System. *Cell Chem Biol.* Sep 17 2020;27(9):1164-1180 e5. doi:10.1016/j.chembiol.2020.06.013
23. Ottis P, Toure M, Cromm PM, Ko E, Gustafson JL, Crews CM. Assessing Different E3 Ligases for Small Molecule Induced Protein Ubiquitination and Degradation. *ACS Chem Biol.* Oct 20 2017;12(10):2570-2578. doi:10.1021/acschembio.7b00485
24. Smith BE, Wang SL, Jaime-Figueroa S, et al. Differential PROTAC substrate specificity dictated by orientation of recruited E3 ligase. *Nature Communications.* 2019/01/10 2019;10(1):131. doi:10.1038/s41467-018-08027-7
25. van den Boom J, Meyer H. VCP/p97-Mediated Unfolding as a Principle in Protein Homeostasis and Signaling. *Mol Cell.* Jan 18 2018;69(2):182-194. doi:10.1016/j.molcel.2017.10.028
26. Noi K, Yamamoto D, Nishikori S, et al. High-speed atomic force microscopic observation of ATP-dependent rotation of the AAA+ chaperone p97. *Structure.* Nov 5 2013;21(11):1992-2002. doi:10.1016/j.str.2013.08.017
27. Olszewski MM, Williams C, Dong KC, Martin A. The Cdc48 unfoldase prepares well-folded protein substrates for degradation by the 26S proteasome. *Commun Biol.* 2019;2:29. doi:10.1038/s42003-019-0283-z
28. Bodnar NO, Rapoport TA. Molecular Mechanism of Substrate Processing by the Cdc48 ATPase Complex. *Cell.* May 4 2017;169(4):722-735.e9. doi:10.1016/j.cell.2017.04.020
29. Hu X, Wang L, Wang Y, et al. RNF126-Mediated Reubiquitination Is Required for Proteasomal Degradation of p97-Extracted Membrane Proteins. *Mol Cell.* Jul 16 2020;79(2):320-331 e9. doi:10.1016/j.molcel.2020.06.023
30. Wentink A, Rosenzweig R. Protein disaggregation machineries in the human cytosol. *Current Opinion in Structural Biology.* 2023/12/01/ 2023;83:102735. doi:<https://doi.org/10.1016/j.sbi.2023.102735>
31. Mukkavalli S, Klickstein JA, Ortiz B, Juo P, Raman M. The p97-UBXN1 complex regulates aggresome formation. *J Cell Sci.* Apr 1 2021;134(7)doi:10.1242/jcs.254201

32. Saha I, Yuste-Checa P, Da Silva Padilha M, et al. The AAA+ chaperone VCP disaggregates Tau fibrils and generates aggregate seeds in a cellular system. *Nature Communications*. 2023/02/02 2023;14(1):560. doi:10.1038/s41467-023-36058-2

33. Ghosh DK, Roy A, Ranjan A. The ATPase VCP/p97 functions as a disaggregase against toxic Huntingtin-exon1 aggregates. *FEBS Lett*. Aug 2018;592(16):2680-2692. doi:10.1002/1873-3468.13213

34. Ye Y, Tang WK, Zhang T, Xia D. A Mighty "Protein Extractor" of the Cell: Structure and Function of the p97/CDC48 ATPase. *Front Mol Biosci*. 2017;4:39. doi:10.3389/fmolb.2017.00039

35. Yeung HO, Kloppsteck P, Niwa H, et al. Insights into adaptor binding to the AAA protein p97. *Biochem Soc Trans*. Feb 2008;36(Pt 1):62-7. doi:10.1042/BST0360062

36. Kloppsteck P, Ewens CA, Förster A, Zhang X, Freemont PS. Regulation of p97 in the ubiquitin-proteasome system by the UBX protein-family. *Biochim Biophys Acta*. Jan 2012;1823(1):125-9. doi:10.1016/j.bbamcr.2011.09.006

37. Meyer H. p97 complexes as signal integration hubs. *BMC Biol*. Jun 13 2012;10:48. doi:10.1186/1741-7007-10-48

38. Stach L, Freemont PS. The AAA+ ATPase p97, a cellular multitool. *Biochem J*. Aug 17 2017;474(17):2953-2976. doi:10.1042/bcj20160783

39. McLellan GL, Goiran T, Yi W, et al. Mfn2 ubiquitination by PINK1/parkin gates the p97-dependent release of ER from mitochondria to drive mitophagy. *Elife*. Apr 20 2018;7doi:10.7554/elife.32866

40. Koyano F, Yamano K, Kosako H, et al. Parkin-mediated ubiquitylation redistributes MITOL/March5 from mitochondria to peroxisomes. *EMBO Rep*. Dec 5 2019;20(12):e47728. doi:10.15252/embr.201947728

41. Galindo-Moreno M, Giraldez S, Saez C, Japon MA, Tortolero M, Romero F. Both p62/SQSTM1-HDAC6-dependent autophagy and the aggresome pathway mediate CDK1 degradation in human breast cancer. *Sci Rep*. Aug 30 2017;7(1):10078. doi:10.1038/s41598-017-10506-8

42. Hirabayashi M, Inoue K, Tanaka K, et al. VCP/p97 in abnormal protein aggregates, cytoplasmic vacuoles, and cell death, phenotypes relevant to neurodegeneration. *Cell Death Differ*. Oct 2001;8(10):977-84. doi:10.1038/sj.cdd.4400907

43. Mizuno Y, Hori S, Kakizuka A, Okamoto K. Vacuole-creating protein in neurodegenerative diseases in humans. *Neurosci Lett*. Jun 5 2003;343(2):77-80. doi:10.1016/s0304-3940(03)00280-5

44. Yang H, Hu HY. Sequestration of cellular interacting partners by protein aggregates: implication in a loss-of-function pathology. *Febs J*. Oct 2016;283(20):3705-3717. doi:10.1111/febs.13722

45. Kobayashi T, Manno A, Kakizuka A. Involvement of valosin-containing protein (VCP)/p97 in the formation and clearance of abnormal protein aggregates. *Genes Cells*. Jul 2007;12(7):889-901. doi:10.1111/j.1365-2443.2007.01099.x

46. Alieva A, Rudenok M, Filatova E, et al. VCP expression decrease as a biomarker of preclinical and early clinical stages of Parkinson's disease. *Sci Rep*. Jan 21 2020;10(1):827. doi:10.1038/s41598-020-57938-3

47. Watts GD, Wymer J, Kovach MJ, et al. Inclusion body myopathy associated with Paget disease of bone and frontotemporal dementia is caused by mutant valosin-containing protein. *Nat Genet*. Apr 2004;36(4):377-81. doi:10.1038/ng1332

48. Falcao de Campos C, de Carvalho M. Distal myopathy and rapidly progressive dementia associated with a novel mutation in the VCP gene: Expanding inclusion body myopathy with early-onset Paget disease and frontotemporal dementia spectrum. *J Clin Neurosci*. Jun 2019;64:8-10. doi:10.1016/j.jocn.2019.03.063

49. Gonzalez MA, Feely SM, Speziani F, et al. A novel mutation in VCP causes Charcot-Marie-Tooth Type 2 disease. *Brain*. Nov 2014;137(Pt 11):2897-902. doi:10.1093/brain/awu224

50. Gonzalez-Perez P, Cirulli ET, Drory VE, et al. Novel mutation in VCP gene causes atypical amyotrophic lateral sclerosis. *Neurology*. Nov 27 2012;79(22):2201-8. doi:10.1212/WNL.0b013e318275963b

51. Alnot JY, Frajman JM. [Chronic ulnar nerve compression syndrome at the elbow. Apropos of 74 cases]. *Ann Chir Main Memb Super*. 1992;11(1):5-13. Syndrome de compression chronique du nerf cubital au niveau du coude. A propos de 74 cas. doi:10.1016/s0753-9053(05)80046-8

52. Huang Q, Figueiredo-Pereira ME. Ubiquitin/proteasome pathway impairment in neurodegeneration: therapeutic implications. *Apoptosis*. Nov 2010;15(11):1292-311. doi:10.1007/s10495-010-0466-z

53. Donaldson KM, Li W, Ching KA, Batalov S, Tsai CC, Joazeiro CA. Ubiquitin-mediated sequestration of normal cellular proteins into polyglutamine aggregates. *Proc Natl Acad Sci U S A*. Jul 22 2003;100(15):8892-7. doi:10.1073/pnas.1530212100

54. Fernandez-Saiz V, Buchberger A. Imbalances in p97 co-factor interactions in human proteinopathy. *EMBO Rep*. Jun 2010;11(6):479-85. doi:10.1038/embor.2010.49

55. Caffrey B, Zhu X, Berezuk A, Tuttle K, Chittori S, Subramaniam S. AAA+ ATPase p97/VCP mutants and inhibitor binding disrupt inter-domain coupling and subsequent allosteric activation. *Journal of Biological Chemistry*. 2021/10/01/ 2021;297(4):101187. doi:<https://doi.org/10.1016/j.jbc.2021.101187>

56. Bodnar NO, Rapoport TA. Molecular Mechanism of Substrate Processing by the Cdc48 ATPase Complex. *Cell*. May 4 2017;169(4):722-735 e9. doi:10.1016/j.cell.2017.04.020

57. Kubala MH, Kovtun O, Alexandrov K, Collins BM. Structural and thermodynamic analysis of the GFP:GFP-nanobody complex. *Protein Sci*. Dec 2010;19(12):2389-401. doi:10.1002/pro.519

58. Pessina F, Giavazzi F, Yin Y, et al. Functional transcription promoters at DNA double-strand breaks mediate RNA-driven phase separation of damage-response factors. *Nat Cell Biol*. Oct 2019;21(10):1286-1299. doi:10.1038/s41556-019-0392-4

59. Zhang L, Geng X, Wang F, et al. 53BP1 regulates heterochromatin through liquid phase separation. *Nat Commun*. Jan 18 2022;13(1):360. doi:10.1038/s41467-022-28019-y

60. Lukas C, Savic V, Bekker-Jensen S, et al. 53BP1 nuclear bodies form around DNA lesions generated by mitotic transmission of chromosomes under replication stress. *Nat Cell Biol*. Mar 2011;13(3):243-53. doi:10.1038/hcb2201

61. Gomez-Isla T, Frosch MP. Lesions without symptoms: understanding resilience to Alzheimer disease neuropathological changes. *Nat Rev Neurol*. Mar 24 2022;doi:10.1038/s41582-022-00642-9

62. Blesa J, Foffani G, Dehay B, Bezard E, Obeso JA. Motor and non-motor circuit disturbances in early Parkinson disease: which happens first? *Nat Rev Neurosci*. Feb 2022;23(2):115-128. doi:10.1038/s41583-021-00542-9

63. Ross CA, Poirier MA. Protein aggregation and neurodegenerative disease. *Nat Med*. Jul 2004;10 Suppl:S10-7. doi:10.1038/nm1066

64. Konstantinidou M, Li J, Zhang B, et al. PROTACs- a game-changing technology. *Expert Opin Drug Discov*. Dec 2019;14(12):1255-1268. doi:10.1080/17460441.2019.1659242

65. Galves M, Rathi R, Prag G, Ashkenazi A. Ubiquitin Signaling and Degradation of Aggregate-Prone Proteins. *Trends Biochem Sci*. Oct 2019;44(10):872-884. doi:10.1016/j.tibs.2019.04.007

66. Gai WP, Yuan HX, Li XQ, Power JT, Blumbergs PC, Jensen PH. In situ and in vitro study of colocalization and segregation of alpha-synuclein, ubiquitin, and lipids in Lewy bodies. *Exp Neurol*. Dec 2000;166(2):324-33. doi:10.1006/exnr.2000.7527

67. Narain Y, Wyttenbach A, Rankin J, Furlong RA, Rubinsztein DC. A molecular investigation of true dominance in Huntington's disease. *J Med Genet*. Oct 1999;36(10):739-46. doi:10.1136/jmg.36.10.739

68. Butler DC, Joshi SN, Genst E, Baghel AS, Dobson CM, Messer A. Bifunctional Anti-Non-Amyloid Component alpha-Synuclein Nanobodies Are Protective In Situ. *PLoS One*. 2016;11(11):e0165964. doi:10.1371/journal.pone.0165964

69. El Turk F, De Genst E, Guilliams T, et al. Exploring the role of post-translational modifications in regulating alpha-synuclein interactions by studying the effects of phosphorylation on nanobody binding. *Protein Sci*. Jul 2018;27(7):1262-1274. doi:10.1002/pro.3412

70. Chatterjee D, Bhatt M, Butler D, et al. Proteasome-targeted nanobodies alleviate pathology and functional decline in an alpha-synuclein-based Parkinson's disease model. *NPJ Parkinsons Dis*. 2018;4:25. doi:10.1038/s41531-018-0062-4

71. Guilliams T, El-Turk F, Buell AK, et al. Nanobodies raised against monomeric α -synuclein distinguish between fibrils at different maturation stages. *J Mol Biol*. Jul 24 2013;425(14):2397-411. doi:10.1016/j.jmb.2013.01.040

72. Lee JW, Bae SH, Jeong JW, Kim SH, Kim KW. Hypoxia-inducible factor (HIF-1)alpha: its protein stability and biological functions. *Exp Mol Med*. Feb 29 2004;36(1):1-12. doi:10.1038/emm.2004.1

73. McGettrick AF, O'Neill LAJ. The Role of HIF in Immunity and Inflammation. *Cell Metab*. Oct 6 2020;32(4):524-536. doi:10.1016/j.cmet.2020.08.002

74. Salvi A, Thanabalu T. Expression of N-WASP is regulated by HIF1alpha through the hypoxia response element in the N-WASP promoter. *Biochem Biophys Rep*. Mar 2017;9:13-21. doi:10.1016/j.bbrep.2016.10.010

75. Yeo EJ. Hypoxia and aging. *Exp Mol Med*. Jun 20 2019;51(6):1-15. doi:10.1038/s12276-019-0233-3

76. Min JH, Yang H, Ivan M, Gertler F, Kaelin WG, Jr., Pavletich NP. Structure of an HIF-1alpha-pVHL complex: hydroxyproline recognition in signaling. *Science*. Jun 7 2002;296(5574):1886-9. doi:10.1126/science.1073440

77. Masoud GN, Li W. HIF-1alpha pathway: role, regulation and intervention for cancer therapy. *Acta Pharm Sin B*. Sep 2015;5(5):378-89. doi:10.1016/j.apsb.2015.05.007

78. Ben Yehuda A, Risheq M, Novoplansky O, et al. Ubiquitin Accumulation on Disease Associated Protein Aggregates Is Correlated with Nuclear Ubiquitin Depletion, Histone De-Ubiquitination and Impaired DNA Damage Response. *PLoS One*. 2017;12(1):e0169054. doi:10.1371/journal.pone.0169054

79. Hyun S, Shin D. Chemical-Mediated Targeted Protein Degradation in Neurodegenerative Diseases. *Life (Basel)*. Jun 24 2021;11(7)doi:10.3390/life11070607

80. Creekmore BC, Watanabe R, Lee EB. Neurodegenerative Disease Tauopathies. *Annu Rev Pathol*. Oct 13 2023;doi:10.1146/annurev-pathmechdis-051222-120750

81. Merchant KM, Cedarbaum JM, Brundin P, et al. A Proposed Roadmap for Parkinson's Disease Proof of Concept Clinical Trials Investigating Compounds Targeting Alpha-Synuclein. *J Parkinsons Dis*. 2019;9(1):31-61. doi:10.3233/JPD-181471

82. Lang AE, Espay AJ. Disease Modification in Parkinson's Disease: Current Approaches, Challenges, and Future Considerations. *Mov Disord*. May 2018;33(5):660-677. doi:10.1002/mds.27360

83. Zhu J, Pittman S, Dhavale D, et al. VCP protects neurons from proteopathic seeding. *bioRxiv*. 2021:2021.07.12.452081. doi:10.1101/2021.07.12.452081

84. Sun X, Gao H, Yang Y, et al. PROTACs: great opportunities for academia and industry. *Signal Transduct Target Ther*. 2019;4:64. doi:10.1038/s41392-019-0101-6

85. Bird RE, Hardman KD, Jacobson JW, et al. Single-chain antigen-binding proteins. *Science*. Oct 21 1988;242(4877):423-6. doi:10.1126/science.3140379

86. Rojas-Fernandez A, Herhaus L, Macartney T, Lachaud C, Hay RT, Sapkota GP. Rapid generation of endogenously driven transcriptional reporters in cells through CRISPR/Cas9. *Sci Rep*. Apr 29 2015;5:9811. doi:10.1038/srep09811

87. Munoz IM, Szyniarowski P, Toth R, Rouse J, Lachaud C. Improved genome editing in human cell lines using the CRISPR method. *PLoS One*. 2014;9(10):e109752. doi:10.1371/journal.pone.0109752

88. Del Rey NL, Balzano T, Martin-Rodriguez L, et al. Lack of Parkinsonian Pathology and Neurodegeneration in Mice After Long-Term Injections of a Proteasome Inhibitor in Olfactory Bulb and Amygdala. *Front Aging Neurosci*. 2021;13:698979. doi:10.3389/fnagi.2021.698979

89. Del Rey NL, Trigo-Damas I, Obeso JA, Cavada C, Blesa J. Neuron types in the primate striatum: Stereological analysis of projection neurons and interneurons in control and parkinsonian monkeys. *Neuropathol Appl Neurobiol*. Mar 10 2022:e12812. doi:10.1111/nan.12812

90. Mirdita M, Ovchinnikov S, Steinegger M. ColabFold - Making protein folding accessible to all. *bioRxiv*. 2021:2021.08.15.456425. doi:10.1101/2021.08.15.456425

91. Jumper J, Evans R, Pritzel A, et al. Highly accurate protein structure prediction with AlphaFold. *Nature*. Aug 2021;596(7873):583-589. doi:10.1038/s41586-021-03819-2

92. Hanzelmann P, Buchberger A, Schindelin H. Hierarchical binding of cofactors to the AAA ATPase p97. *Structure*. Jun 8 2011;19(6):833-43. doi:10.1016/j.str.2011.03.018

93. Pan M, Zheng Q, Yu Y, et al. Seesaw conformations of Npl4 in the human p97 complex and the inhibitory mechanism of a disulfiram derivative. *Nat Commun*. Jan 5 2021;12(1):121. doi:10.1038/s41467-020-20359-x

94. Emsley P, Lohkamp B, Scott WG, Cowtan K. Features and development of Coot. *Acta Crystallogr D Biol Crystallogr*. Apr 2010;66(Pt 4):486-501. doi:10.1107/S0907444910007493

Figure-1

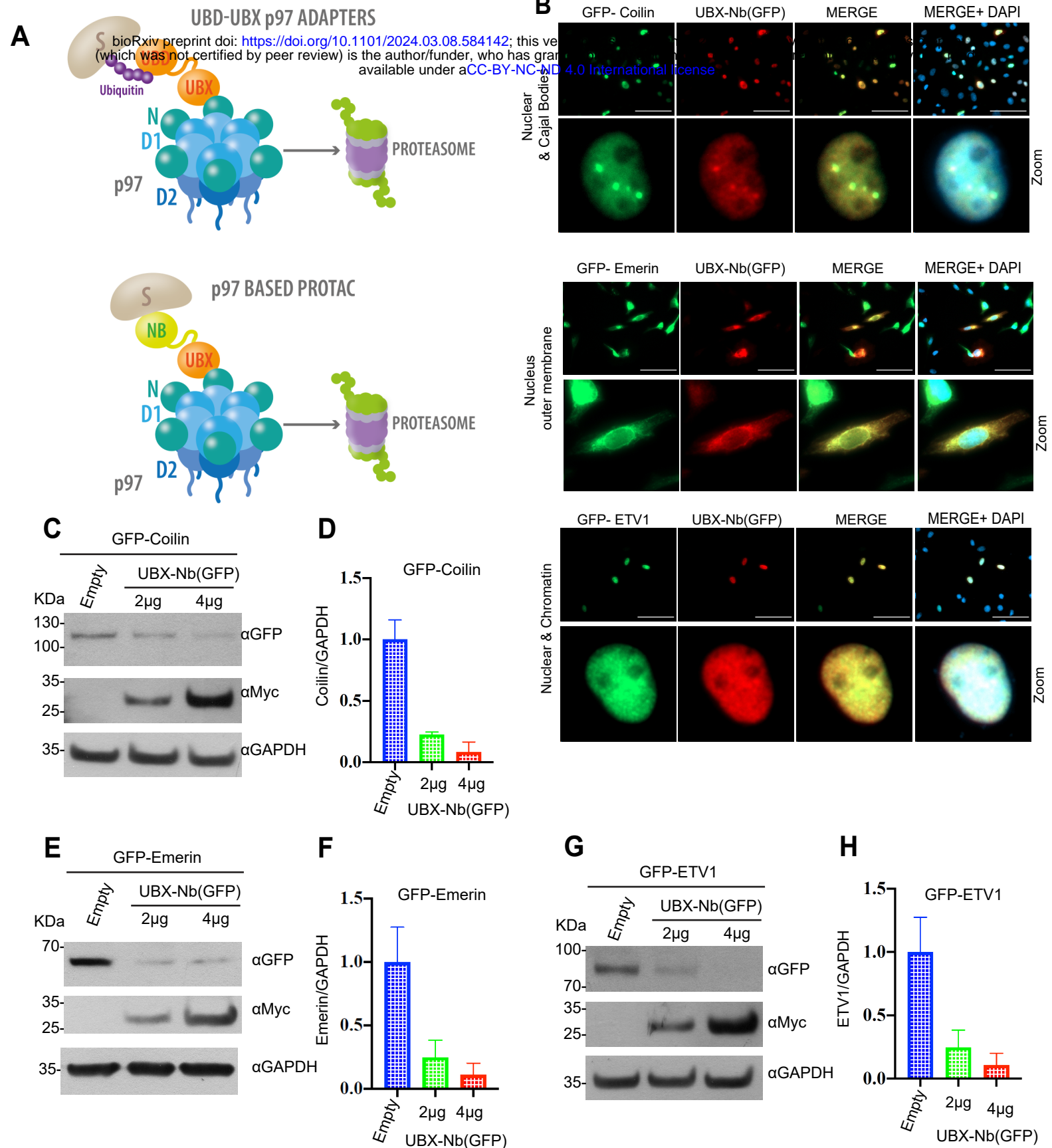
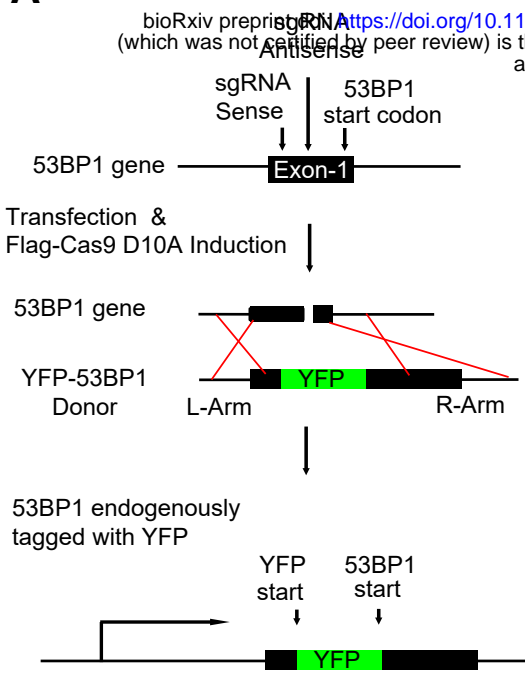
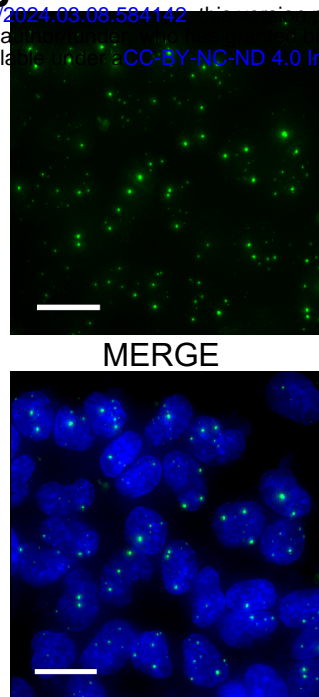


Figure-2

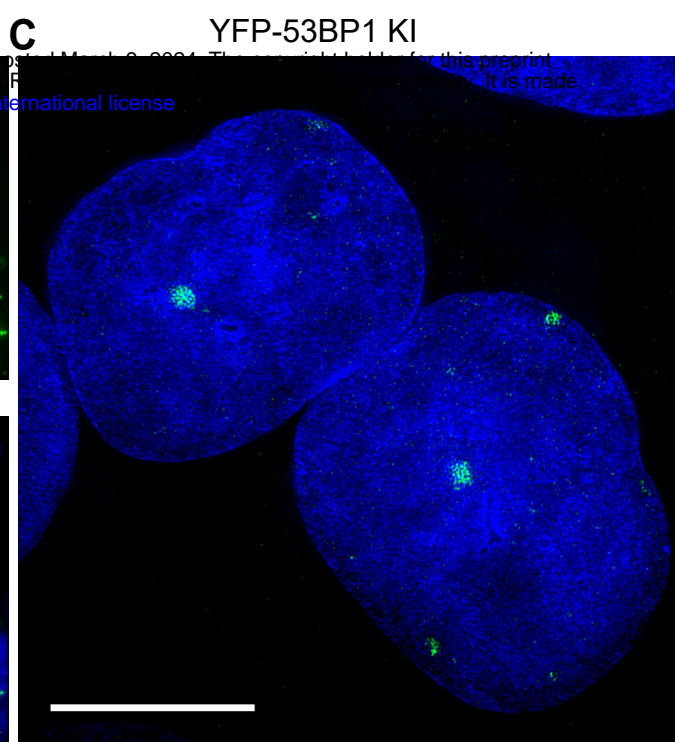
A



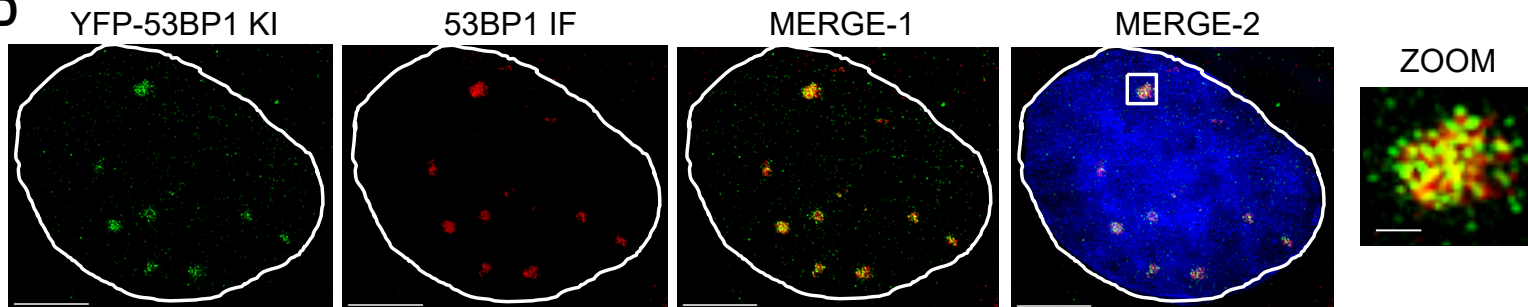
B YFP-53BP1 KI



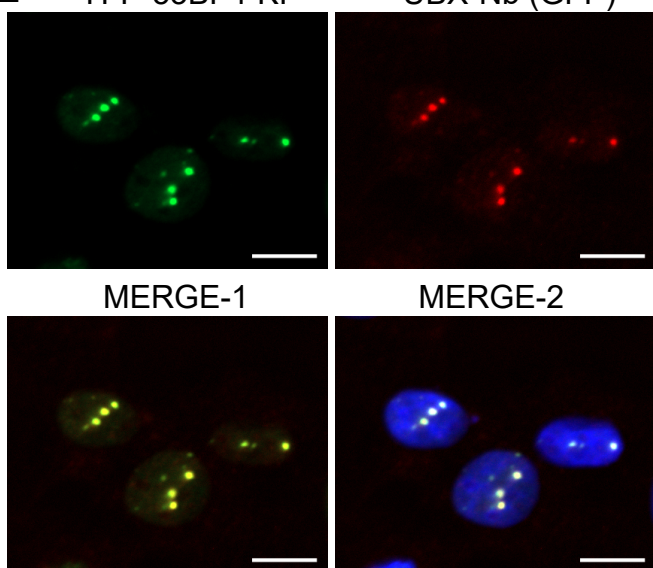
C



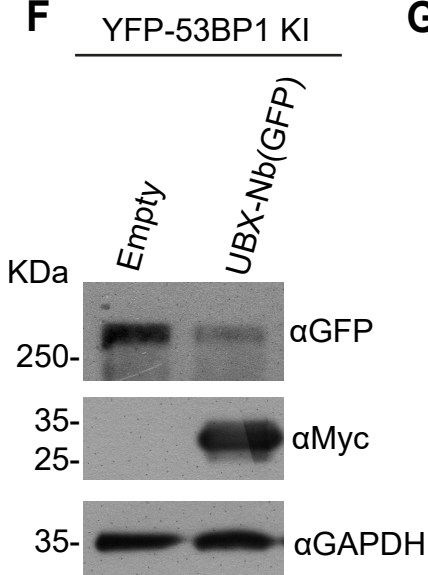
D



E



F



G

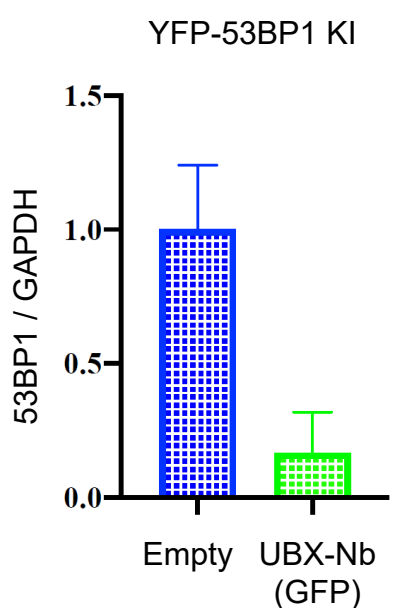
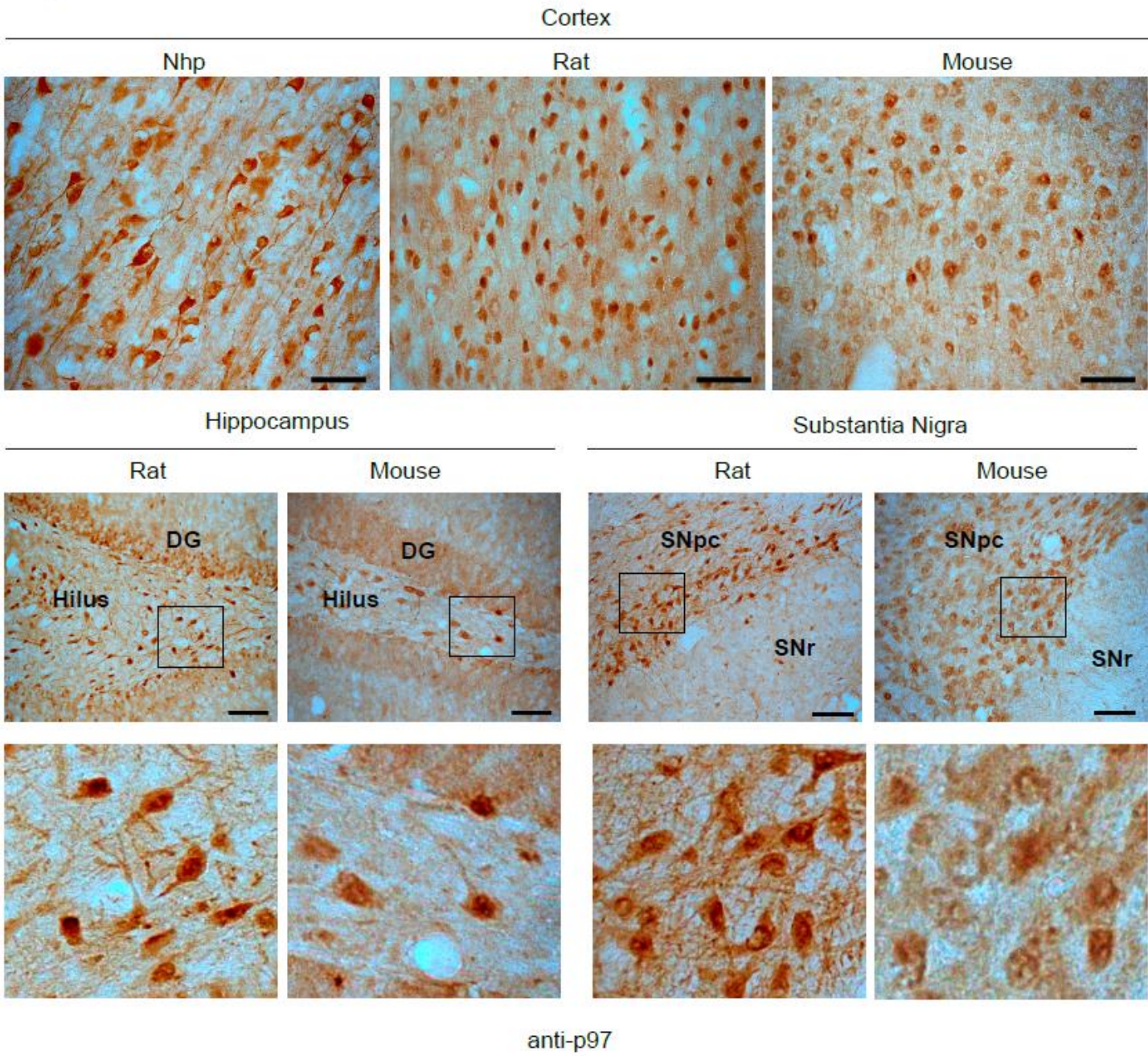


Figure-3



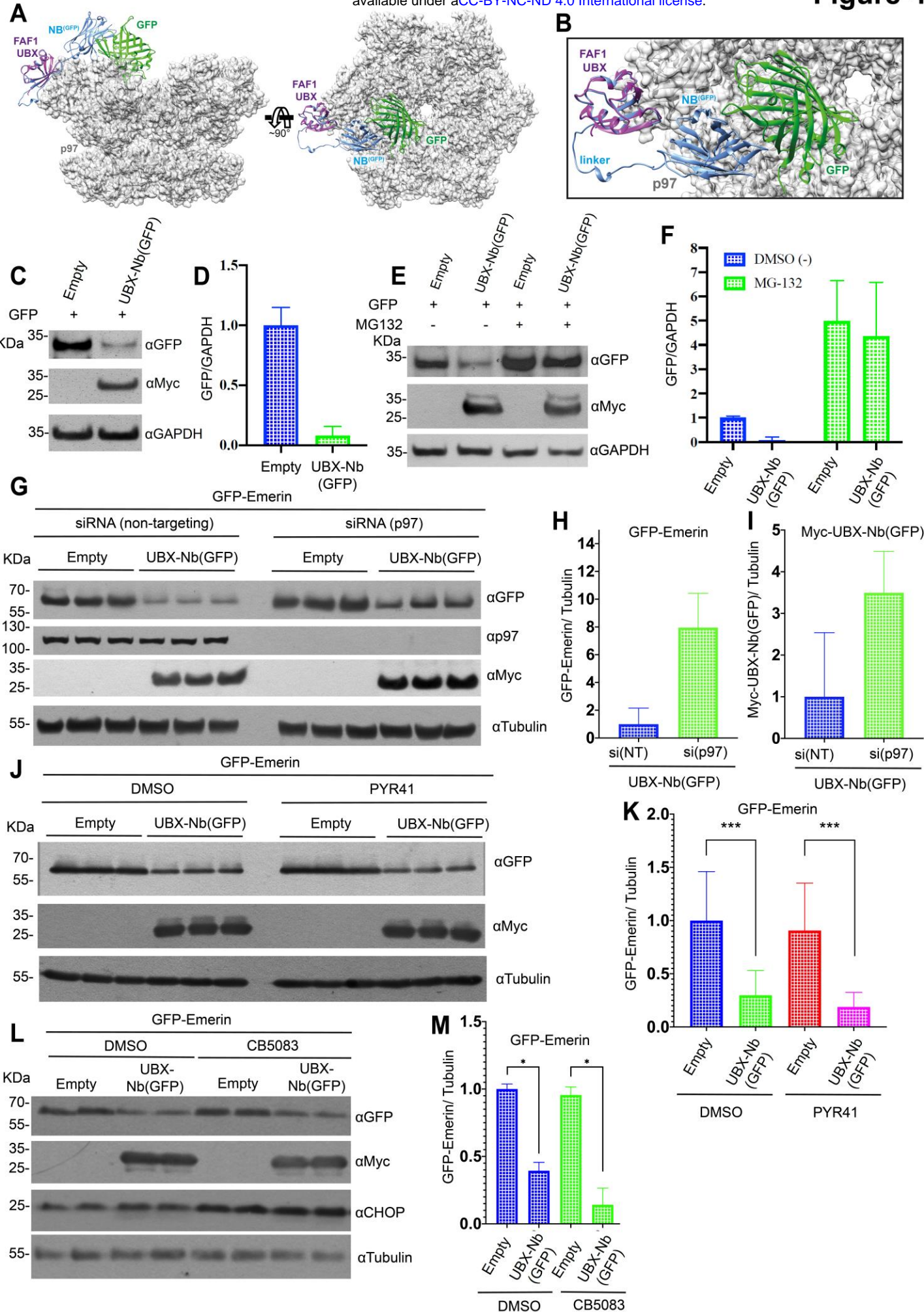


Figure 5

bioRxiv preprint doi: <https://doi.org/10.1101/2024.03.08.584142>; this version posted March 9, 2024. The copyright holder for this preprint (which was not certified by peer review) is the author/funder, who has granted bioRxiv a license to display the preprint in perpetuity. It is made available under aCC-BY-NC-ND 4.0 International license.

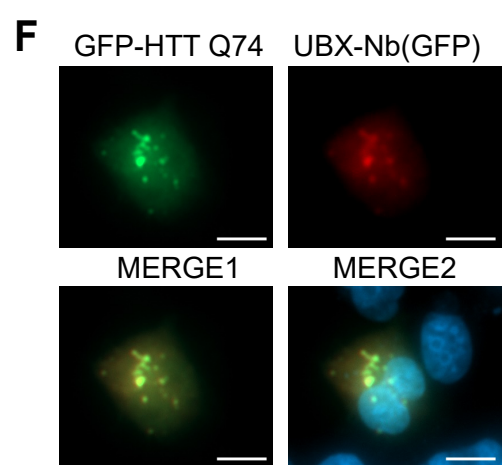
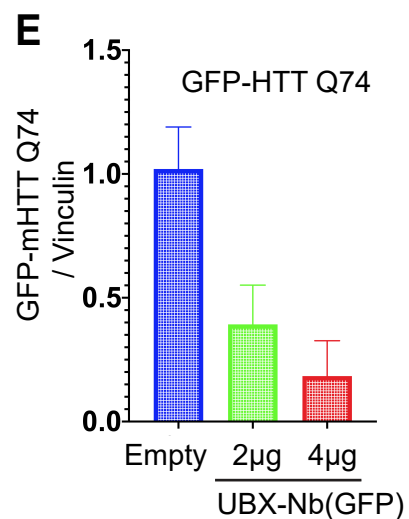
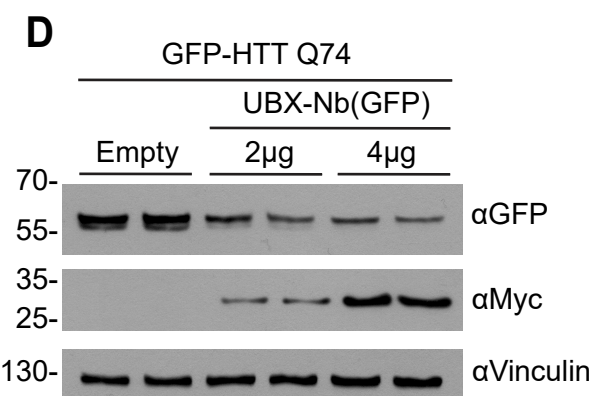
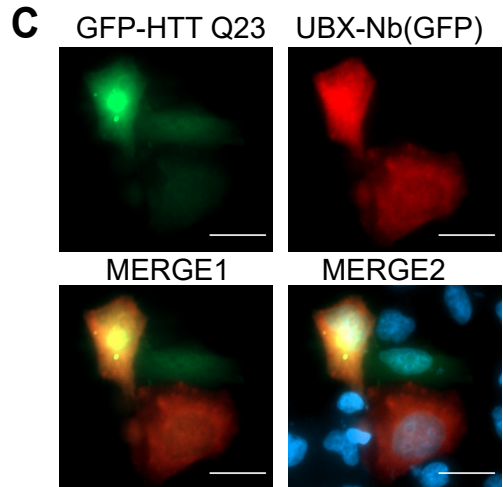
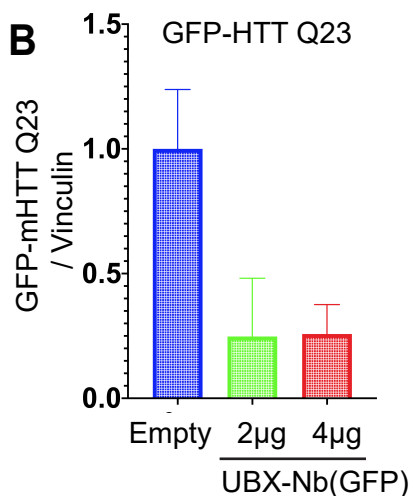
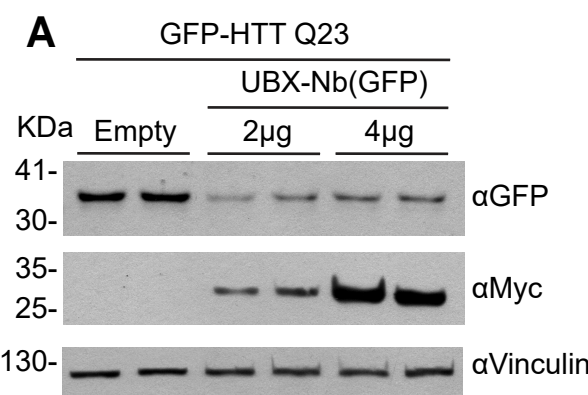
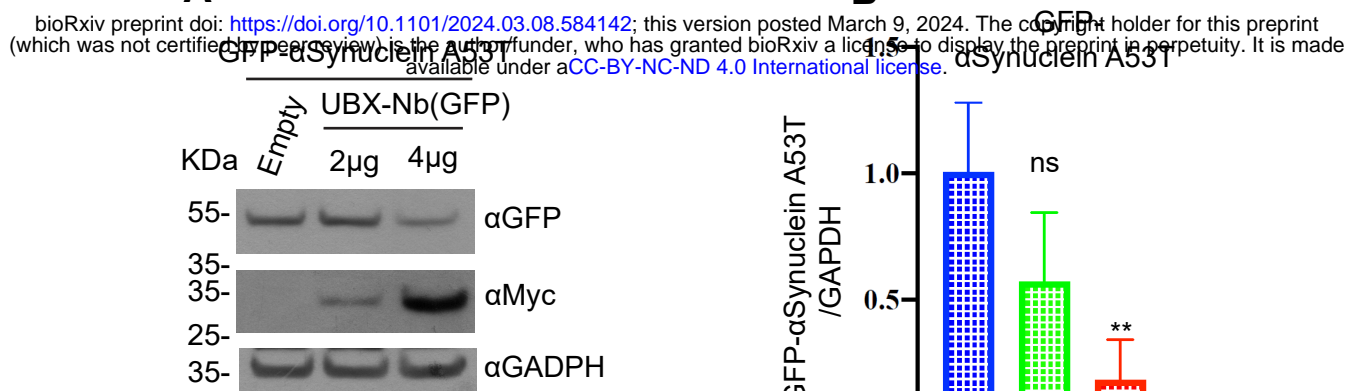
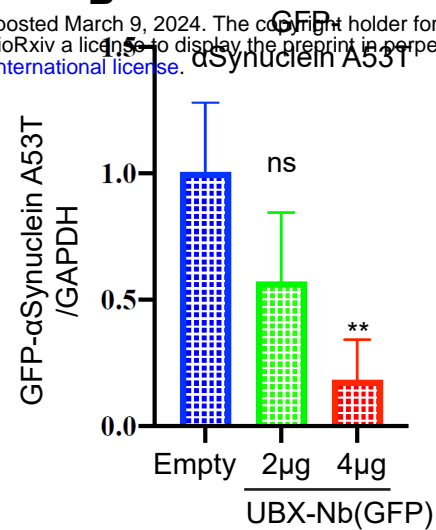


Figure-6

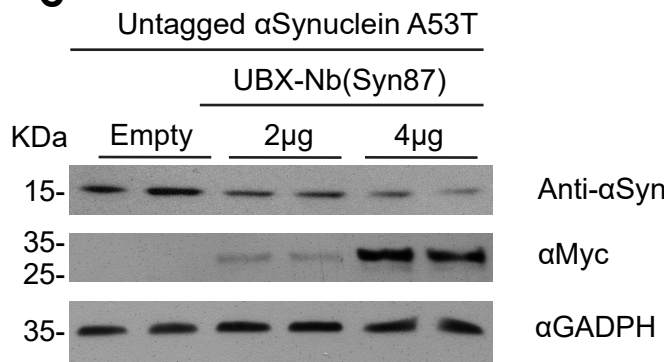
A



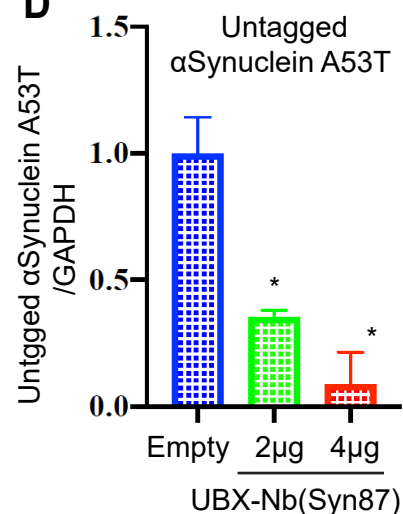
B



C



D



E

